Multi-Scale Biomechanical Characterization of Human Liver and Spleen

Andrew Kemper, Anthony Santago, Jessica Sparks, Craig Thor,
H. Clay Gabler, Joel Stitzel, and Stefan Duma
Virginia Tech – Wake Forest, Center for Injury Biomechanics
United States of America
Paper Number 11-0195

ABSTRACT

The purpose of this study is to present a multi-scale approach for the biomechanical characterization of the human liver and spleen. A four step approach was taken to quantify the injury mechanism, biomechanical response, and rate dependent constitutive material models for each organ. First, the CIREN and NASS-CDS databases were examined to determine the crash characteristics which result in liver and spleen injuries. From this data, the injury mechanism relative to loading directions and loading rates could be approximated. Second, whole fresh human organs were tested with in 48 hours of death using indenter-style compression tests. Sub-failure tests, up to 20% compression, were performed at multiple loading rates, followed by a failure test. Third, fresh human organs were processed into either dog-bone tension coupons or cylindrical compression coupons and tested within 48 hours of death at multiple strain rates to the point of failure. Fourth, an optimization routine and FEM of the coupons tests was developed to determine the best constitutive model for each organ. The data from this study shows that the response of human liver and spleen is both non-linear and rate dependant. It is anticipated that the data from this research will enhance the understanding of internal organ injuries and provide a foundation for future human internal organs finite element models.

INTRODUCTION

Motor vehicle collisions (MVCs) commonly result in serious blunt abdominal injuries [Mackenzie et al., 2003]. Although abdominal injuries account for only 3-5% of all injuries observed in MVCs, they comprise 8% of AIS 3+ injuries, 16.5% of AIS 4+ injuries and 20.5% of AIS 5+ injuries [Bondy, 1980; Rouhana and Foster, 1985; Elhagediab and Rouhana, 1998; Augenstein et al., 2000]. Although it has been demonstrated that internal organ injuries account for a considerable portion of injuries in automotive crashes, previous studies pre-date the implementation of advanced safety restraint technologies such as: depowered airbags, seatbelt load limiters, and seatbelt pretensioners.

Currently, no crash test dummies used to assess injury risk in MVCs are equipped to represent individual solid abdominal organs located asymmetrically in the human abdomen [Tamura et al., 2002]. Consequently, finite element models (FEMs) are becoming an integral tool in the reduction of automotive related abdominal injuries. However, the response of these models must be locally and globally validated based on appropriate biomechanical data in order to accurately assess injury risk. Furthermore, since FEMs allow for the prediction of injury based on the calculation of physical variables mechanically related to injury, such as stress and strain, the establishment of tissue level tolerance values is critical for the accurate prediction of injuries [Moorcroft et al., 2003; Stitzel et al., 2005a; Stitzel et al., 2005b; Takhounts et al., 2008].

Several biomechanical studies have evaluated the mechanical response and injury tolerance of the internal organs by conducting compression tests on intact animal or human cadaver organs [Melvin et al., 1973; Trollope et al., 1973; Wang et al., 1992; Kerdok et al., 2006; Sparks et al., 2007]. Although these studies provide significant contributions to the literature and valuable organ level validation data, they are limited in their ability to accurately quantify localized stress and strain essential for local FEM validation.

In order to directly quantify the material properties of biological tissue, tension and compression testing must be conducted on isolated tissue coupons. There have only been a few studies which have investigated the compressive material properties of liver or spleen by performing compression tests on isolated samples [Tamura et al., 2002; Nasseri et al., 2003; Roan and Vemaganti, 2007; Mazza et al., 2007]. A number of studies have investigated the failure properties of liver by performing tension tests on isolated samples of

liver or spleen tissue [Yamada, 1970; Uehara, 1995; Stingl et al., 2002; Hollenstein et al., 2006; Santago et al. 2009a; Santago et al., 2009b] Although these studies have provided considerable insight into the factors that affect the material response of the liver and spleen parenchyma, these studies have been limited to testing of animal tissue, sub-failure loading, or a single loading rate.

The purpose of the paper is to present a multi-scale approach to characterize injuries and material properties of the human liver and spleen. This approach consists of four parts: determine the crash characteristics which result in liver and spleen injuries, perform indenter-style compressive impacts to intact whole human organs, conduct tension and compression material tests on isolated specimens of human liver and spleen parenchyma at multiple loading rates, and develop a method to obtain accurate FEMs from the tissue level tests.

METHODS AND PRELIMINARY RESULTS

Whole Body Data Analysis

Multiple resources were utilized to perform data-driven analyses of injuries to the heart and great vessels, lungs, liver, and spleen. The National Automotive Sampling System - Crashworthiness Data System (NASS-CDS) was utilized to determine the distribution and mechanisms of thoracic organ injury. The liver and spleen were included as thoracic organs because they are partially protected by the rib cage and they are among the most frequently injured internal organs. For this analysis, only buckled, front seat occupants in vehicles of model year 1998 or later were included. Crash modes were limited to frontal crashes and rollovers were excluded. The distributions in Figures 1, 2, and 3 were published in Thor (2008).

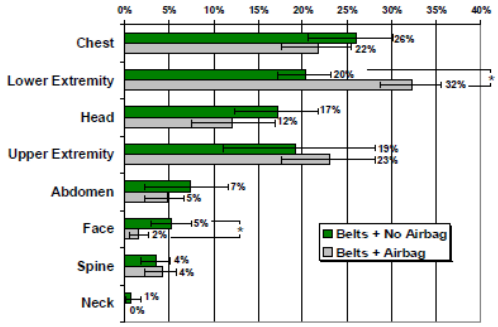

Figure 1: Distribution of MAIS 3+ injuries by body regions (weighted).

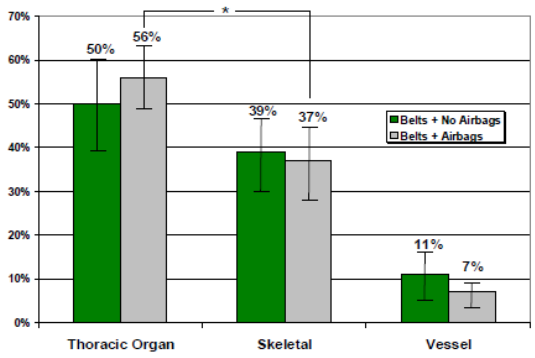

Figure 2: Distribution of AIS 3+ thoracic injuries by tissue type (weighted).

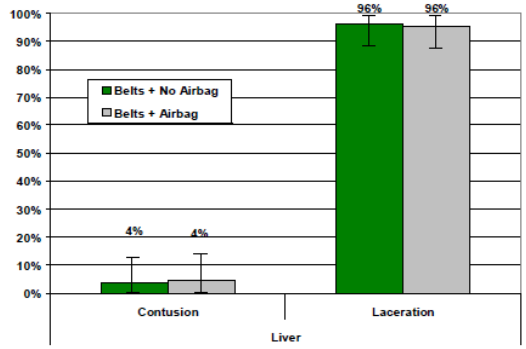

Figure 3: Distribution of AIS3+ liver injuries by lesion type (weighted).

The Virginia Tech – Wake Forest University CIREN database was utilized to determine the crash characteristics and involved physical components for cases which resulted in a liver or spleen injury. It was found that 12.5% (10 of 80 patients) of CIREN study patients experienced liver injuries and 20% (16 of 80 patients) experienced spleen injuries.

For each of the aforementioned injury groups, the crash characteristics were determined (Figures 4 and 5). Often, case occupants sustained injuries in several anatomical categories so each injury listing is not exclusive. The involved physical components assigned to each bio-tabbed injury were also determined. The majority of bio-tabbed liver injuries were attributed to seatbelt loading. The majority of bio-tabbed spleen injuries were attributed to loading from the door.

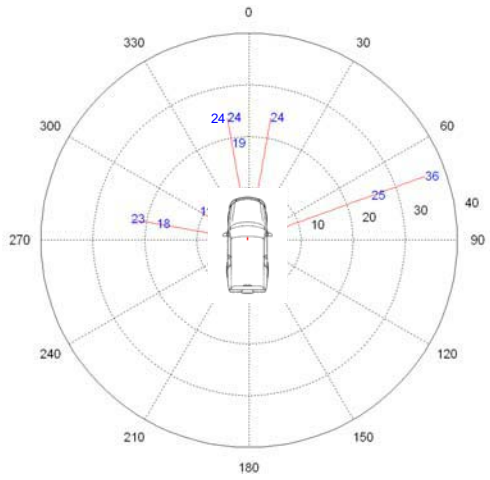

Figure 4: Radial plot of crash Delta-V and PDOF for CIREN cases with liver injuries.

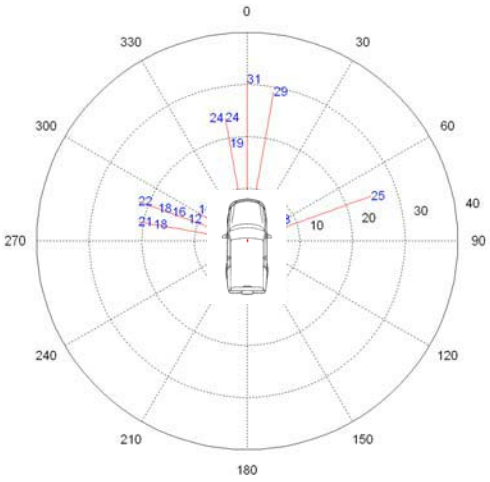

Figure 5: Radial plot of crash Delta-V and PDOF for CIREN cases with spleen injuries.

Organ and Tissue Testing

Organ Procurement and Preservation- In order to obtain accurate material properties it is imperative to test the organs as quickly as possible after subject death. A procurement protocol was developed in order to limit degradation of the organs (Figure 6). Each organ was obtained within 36 hours of death and tested within 48 hours of death to minimize the adverse effects of tissue degradation. An age limit of 80 was set for each subject. All donors were screened to avoid any medical issues that might affect the mechanical properties of the liver or spleen, such as hepatitis and abdominal cancer. It should be noted that the organs were not frozen at any point between the time of death and testing since it has been shown that freezing significantly affects the tensile material properties of the liver parenchyma [Santago et al., 2009b]. In order to preserve the tissue between the time of procurement and specimen preparation, the organs were immersed in Dulbecco's Modified Eagle Medium (DMEM), which is a tissue culture medium, and chilled with wet ice.

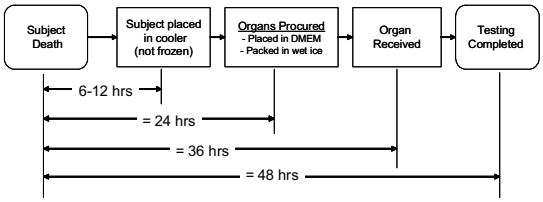

Figure 6: Organ procurement testing time-line.

Whole Organ Testing- The primary component of the indenter-style whole organ compression experimental setup was a high rate servo-hydraulic material testing system (MTS Systems Corporation, MTS-810, Eden Prairie, MN) (Figures 6 and 7). A load cell (Interface 1210-AF-500lbf, Scottsdale, AZ) was attached into the MTS piston. An accelerometer (Endevco 7264B, 2000 g, San Juan Capistrano, CA) was attached to the load cell, and was used to inertially compensate the force. The piston displacement was measured with the MTS internal linear variable differential transformer (LVDT) and a potentiometer (Space Age Control, 160-1705, 540mm, Palmdale, CA) attached to the MTS piston. A cylindrical polypropylene impactor (Dia.=3.81 cm) attached to the load cell was used to load the organs. It should be noted that the edge of the impactor tip was chamfered (r =10 mm).

Each organ was placed on a rigid flat plate, covered with a Teflon© sheet, and aligned underneath the impactor (Figures 7 and 8). A gravity-fed perfusion system was used to pressurize the arterial and venous systems of the organ to simulate physiological conditions [Kerdok et al., 2006; Sparks et al., 2007]. A static pressure of 100 mmHg was utilized for the hepatic artery and splenic artery, while a static pressure of 9 mmHg was utilized for the hepatic vein and splenic vein [Sparks et al., 2007]. The perfusion fluid was heated to approximately 98°F to simulate physiological conditions. A contact switch, consisting of copper tape on the impactor tip and a thin wire placed on the organ, was used to determine the time of initial contact.

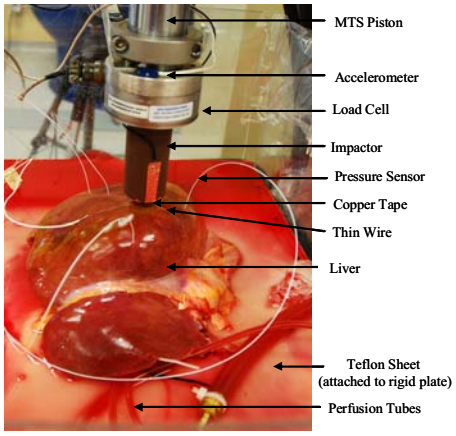

Figure 7: Whole liver on test apparatus.

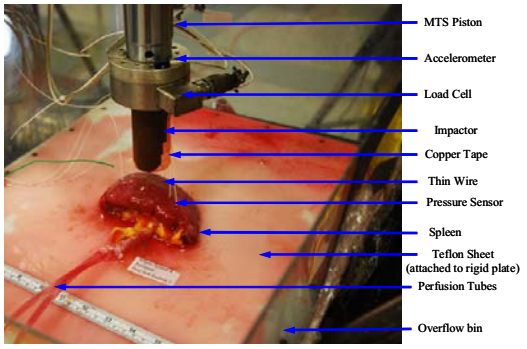

Figure 8: Whole spleen on test apparatus.

Once the perfused organ was positioned on the test setup, the organ and impactor were scanned using a FaroArm (FARO, Platinum 8Ft Arm and P1 Scanner, Switzerland) to obtain the three dimensional surface geometry (Figures 9 and 10). It should be noted that the organ was perfused with heated fluid for approximately one hour prior to scanning. Obtaining the three dimensional surface geometry of each organ allows for the development and validation of organ specific FEMs.

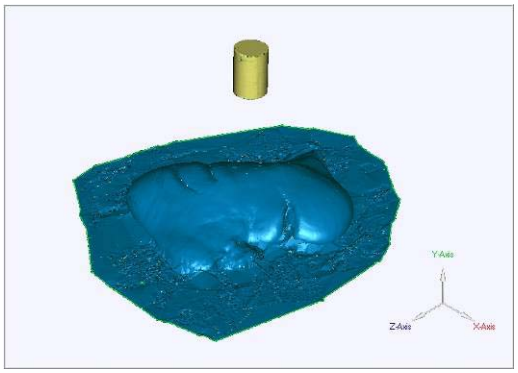

Figure 9: 3D surface geometry of a liver (blue) and impactor (gold).

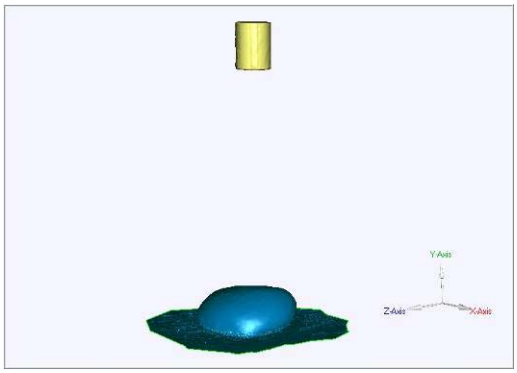

Figure 10: 3D surface geometry of a spleen (blue) and impactor (gold).

A series of impacts were performed on each organ. Each organ was allowed to sit for approximately 10 minutes between each test to allow time for the organ to recover after the impacts. First, 15 preconditioning cycles were performed using a maximum deflection of 20% of the organ height at a loading rate of 0.2Hz, which is the rate of normal breathing. It should be noted that the height of the organ at the point of impact decreased after preconditioning. A series of three impacts were then performed at 2mm/sec, 20mm/sec, and 200mm/sec to a depth of 20% of the organ height measured prior to preconditioning. The sub-failure loading performed on 3 perfused livers is provided as an example (Figure 11). Finally, a failure impact was performed at 2000mm/sec. However, the failure tests are not presented in this paper. The whole liver force versus deflection curves show that the compressive response was non-linear and rate dependent.

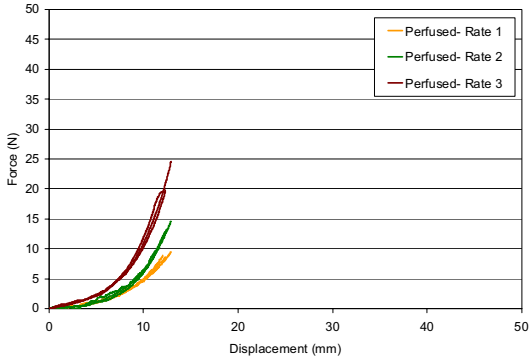

Figure 11: Liver sub-failure loading at multiple loading rates. (Note: Data cut at 14% compression)

Tissue Level Tension Testing- Uniaxial tension tests were conducted using "dog-bone" shaped tension samples of constant thickness. A custom blade assembly and slicing jig were used to obtain constant thickness slices of liver and spleen parenchyma (Figure 12). The blade assembly consisted of multiple 48.3 cm long razor blades spaced such that the tips of the blades were 5 mm apart. The slicing jig was an aluminum fixture, designed to securely hold a block of tissue, with vertical slots spaced 5 mm apart to act as guides for the blades. To generate tissue slices, a square block of tissue was first cut from the parenchyma of the liver or spleen and placed in the slicing jig. The blades were then aligned in the blade guides on the slicing jig. The slicing was performed in one smooth slow pass through the tissue while minimizing downward force in order to avoid damaging or deforming the tissue. The tissue slices were then immersed in a bath of DMEM to maintain specimen hydration.

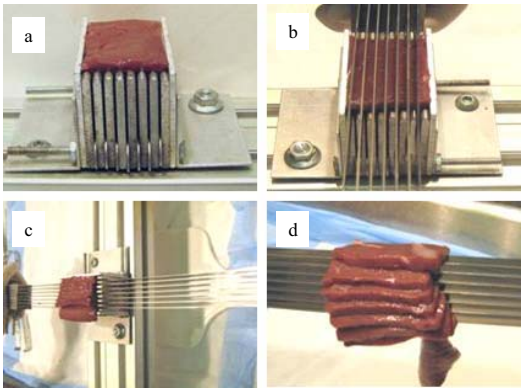

Figure 12: Specimen slicing methodology.

A custom stamp and stamping base were used to obtain "dog-bone" shaped specimens commonly used for uniaxial tension testing. The geometry of the dog-bone was designed to ensure that the specimen would fail in the gage length, which had a constant width and thickness. Prior to stamping, a template was used to position the tissue slice on the stamping base in order to obtain a specimen devoid of any visible vasculature or defects (Figure 13). The stamp was then placed over the tissue slice and lightly struck several times in order to cut the tissue into the desired shape (Figure 13). After stamping, the dog-bone samples were then immersed in a bath of DMEM to maintain specimen hydration.

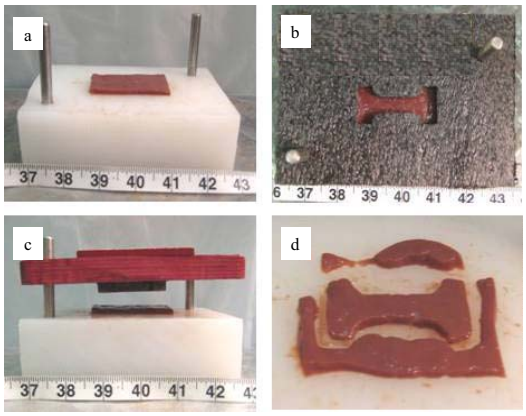

Figure 13: Tension specimen stamping methodology.

The primary component of the tension experimental setup was a custom designed uniaxial dynamic tensile testing system (Figure 14). The entire experimental setup was contained in an environmental test chamber heated to 37°C. The testing system consisted of two motor driven linear stages (Parker Daedal MX80S, Irwin, PA) mounted to a vertically oriented aluminum plate. Each of the linear stages was instrumented with a single-axis load cell (Interface, WMC Miniature-22.24N**,** Scottsdale, AZ) and accelerometer (Endevco 7264B, 2000 G, San Juan Capistrano, CA). The system was operated with a multi-axis controller (Parker ACR9000, Irwin, PA), which provided synchronized motion of both linear stages, and a motor driver (Parker ViX, Irwin, PA). The testing system placed a tensile load on the test specimen by simultaneously moving the top and bottom grips away from one another at a constant velocity.

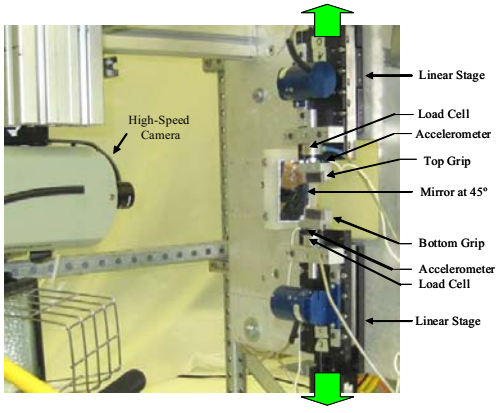

Figure 14: Uniaxial tension experimental setup**.**

For tension testing, a detailed mounting procedure was developed in order to minimize variations in initial specimen preload and the adverse affects of shear due to improper specimen alignment. Immediately prior to mounting the specimens on the experimental setup, the specimens were immersed in a bath of DMEM heated to 37°C. To mount the specimens the top grip assembly was first removed from the experimental setup and laid flat on a table top. The specimen was aligned on the top grip so that the main axis of the specimen coincided with the centerline of the load train and then clamped in place. Sandpaper was placed on the clamping surfaces to ensure that the specimens would not slip during loading. After clamping, the top grip assembly was then attached to the experimental setup and the specimen was allowed to hang in 1 g of tension and then clamped into the bottom grip. By allowing the specimens to hang under their own weight during the clamping process, all specimens had a minimal but consistent preload.

Once the coupons were mounted, side view and back view pre-test pictures were taken with high resolution digital cameras in order to obtain initial width and thickness measurements at the failure locations (Figures 15). Finally, equally spaced optical markers were placed on the gage length in view of the high-speed camera. In order to investigate rate dependence, each specimen was pulled to failure at one of four desired strain rates: 0.01 s^{-1}, 0.1 s^{-1}, 1.0 s^{-1}, or 10.0 s^{-1}.

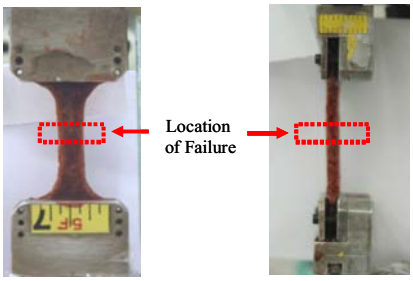

Figure 15: Pre test width and thickness images for the tension tests.

For a tension test to be deemed acceptable, the location of the failure must have occurred in the gage length of the specimen. Therefore, specimens which tore next to the grip or pulled out of either grip were not included in the data set. Failure was defined as the point at which the failure tear initiated in the high-speed video. If the initiation of the failure tear could not be observed in the video, then failure was defined as the point of peak load preceding a significant decrease in the load. Local stress was calculated from the measured displacement between the closest optical markers surrounding the location of the failure tear, which was quantified using motion analysis software. Local stress was calculated based on the inertially compensated force and the original cross-sectional area at the location of the failure. Characteristic averages were developed for each loading rate (Lessley et al. 2004).

The stress versus strain curves for specimens tested at approximately 0.1 s^{-1} are provided as examples, along with the corresponding characteristic average and standard deviations (Figures 16 and 17). The stress versus strain curves show that the tensile response was non-linear for both liver and spleen tensile specimens. Although the 1 g initial condition used in the current study provided a consistent initial state of strain for all specimens, the effect of this condition on the toe region of the stress versus strain curves should be addressed and quantified in future studies.

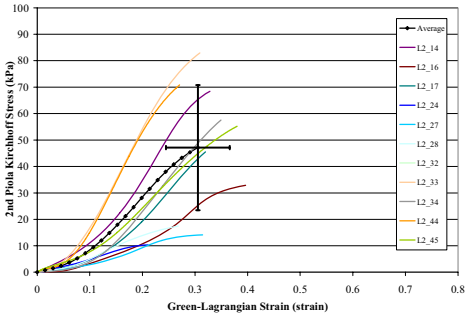

Figure 16: Human liver parenchyma response in uniaxial tension at ~0.1 s^{-1}.

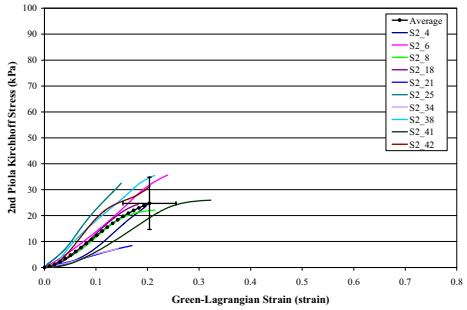

Figure 17: Human spleen parenchyma response in uniaxial tension at ~0.1 s^{-1}.

The results from the liver and spleen tension tests demonstrate rate dependence, with strain decreasing and stress increasing with each increasing strain rate (Figures 18 and 19). The results also show that the tensile failure stress and strain were considerably higher for the liver parenchyma compared to that of the spleen.

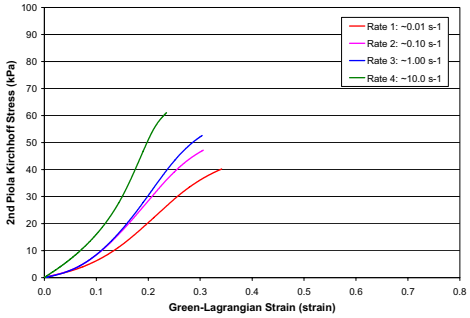

Figure 18: Characteristic averages for human liver parenchyma in uniaxial tension.

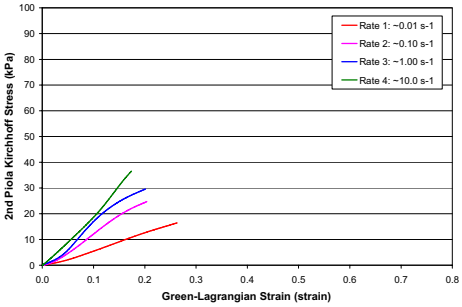

Figure 19: Characteristic averages for human spleen parenchyma in uniaxial tension.

Tissue Level Compression Testing- Uniaxial compression tests were performed on cylindrical compression samples of constant thickness. As with the tension testing, the same custom blade assembly and slicing jig were used to obtain constant thickness slices of liver and spleen parenchyma. However, the 48.3 cm long razor blades were spaced such that the tips of the blades were 10 mm apart for compression samples. After slicing, the samples were immersed in a bath of DMEM to maintain specimen hydration.

A custom cylindrical cutting tool and stamping base were used to obtain cylindrical shaped specimens commonly used for uniaxial compression testing (Figure 20). The custom cylindrical cutting tool was a sharpened, hollow, metal tube (I.D. = 25.4 mm). Prior to cutting, a template was used to position the tissue slice on the stamping base in order to obtain a specimen devoid of any visible vasculature or defects. The cutting was performed by slowly rotating cutting tool about the long axis, while applying minimal downward force in order to avoid tearing and deformation. After cutting, the samples were immersed in a bath of DMEM to maintain specimen hydration.

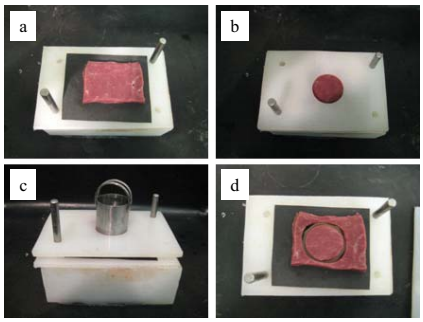

Figure 20: Compression specimen cutting methodology.

The primary component of the compression experimental setup was a high rate servo-hydraulic material testing system (MTS Systems Corporation, MTS-810, Eden Prairie, MN) (Figure 21). A load cell (Interface 1210-AF-500lbf, Scottsdale, AZ) was attached to a base plate, and the testing basin was attached to the top of the load cell. A load cell (Interface 1210-AF-500lbf, Scottsdale, AZ) was attached between the MTS piston, and the impacting surface. Both the reaction and impacting surfaces were constructed of polypropylene. An accelerometer (Endevco 7264B, 2000 g, San Juan Capistrano CA) was attached to the impacting surface, and was used to inertially compensate the impactor force. The piston displacement was measured with the MTS internal LVDT and a potentiometer (Space Age Control, 160-1705, 540mm, Palmdale, CA) attached to the MTS piston.

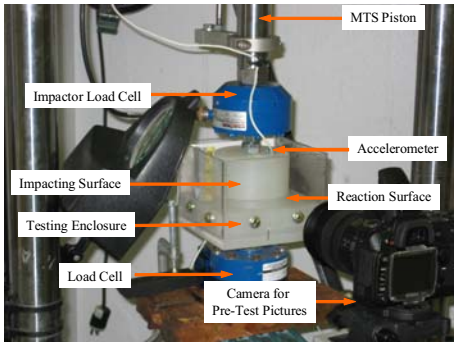

Figure 21: Uniaxial compression experimental setup.

Immediately prior to placing the specimens on the experimental setup, the specimens were immersed in a bath of DMEM heated to 37°C. A silicon spray lubricant was applied to each loading surface before each specimen was placed on the test setup to minimize friction between the specimen and each loading surface. After allowing the specimen to soak in the heated DMEM bath for several minutes, the specimen was removed and placed in the center of the reaction surface. Side view and top view pre-test pictures were taken to determine initial specimen area and initial specimen height (Figure 22). The impacting surface was then moved into position 13 mm above the maximum stroke to give the impactor time to accelerate to the desired velocity before contacting the sample (Figure 28).

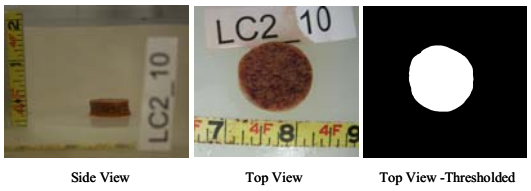

Figure 22: Pre-test area and thickness images for the compression tests.

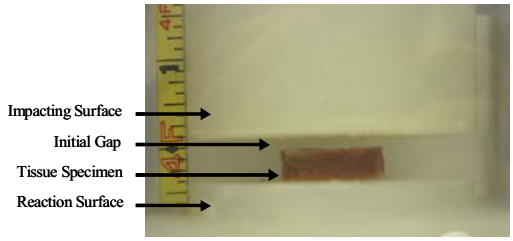

Figure 23: Pre-test image showing initial gap.

In order to investigate rate dependence, each specimen was compressed to failure at one of four desired strain rates: 0.01 s^{-1}, 0.1 s^{-1}, 1.0 s^{-1}, or 10.0 s^{-1}. Failure was defined as the fist major inflection point in the force time history (Figure 24). Strain was calculated based on the displacement of the MTS piston and initial specimen height. Stress was calculated based on the inertially compensated force and the original cross-sectional area, which was calculated using a custom Matlab code to analyze the thresholded top view image. Characteristic averages were developed for each loading rate in tension and compression (Lessley et al. 2004).

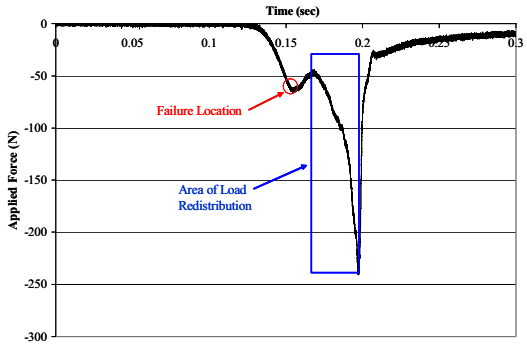

Figure 24: Typical force curve for compression specimens.

The stress versus strain curves for specimens tested at the approximately 1.0 s^{-1} are provided as examples, along with the corresponding characteristic average and standard deviations (Figures 25 and 26). The stress versus strain curves show that the compressive response was non-linear for both liver and spleen compressive specimens.

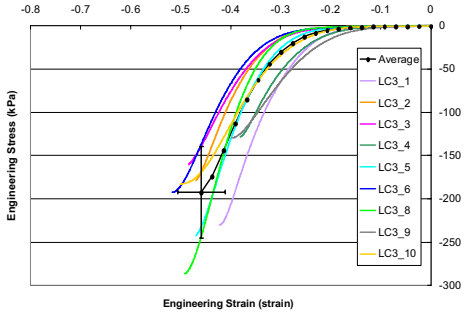

Figure 25: Human liver parenchyma response in uniaxial compression at ~1.0 s^{-1}.

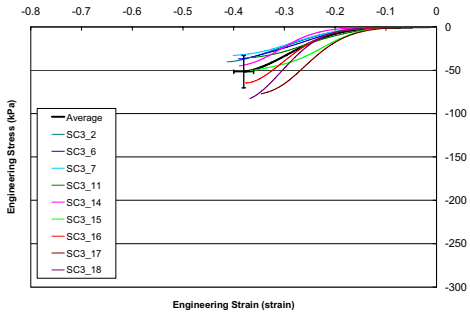

Figure 26: Human spleen parenchyma response in uniaxial compression at ~1.0 s^{-1}.

The results from the liver and spleen compression tests demonstrate rate dependence, with strain decreasing and stress increasing with each increasing strain rate (Figures 27 and 28). The results also show that the compressive failure stress was considerably higher for the liver parenchyma compared to that of the spleen.

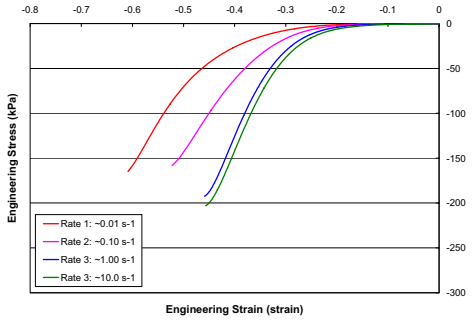

Figure 27: Characteristic averages for human liver parenchyma in uniaxial compression.

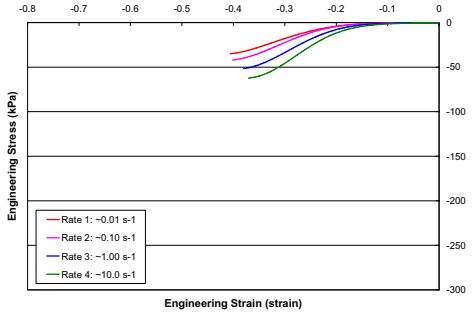

Figure 28: Characteristic averages for human spleen parenchyma in uniaxial compression.

Material Model Optimization Method

The overall approach to model development and optimization is shown in Figure 29. It involves experimental data interpretation and conditioning, simulation, and optimization steps outlined here.

Raw data processing: Raw data from the tensile tests are loaded and separated into different strain rate categories. Each strain rate has multiple series that consist of data from individual tests. Two graphs are produced for each series: displacement versus time and force versus time. Data before t=0 is truncated, and then normalization of the data is performed. The displacements are normalized by initial gauge length into stretches and the forces are normalized by initial cross-sectional area into stress. The initial cross sectional area for each series is calculated by multiplying the thickness by the gauge width. By normalizing both the displacement and the force, the series can then be combined to get a characteristic average for each strain rate. In addition to a characteristic average for each strain rate, a global characteristic average can be acquired to estimate initial material parameters.

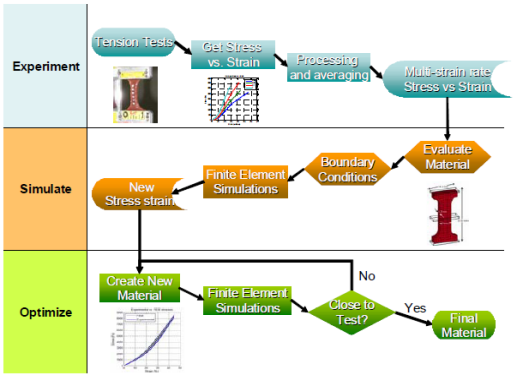

Figure 29: Optimization for finite element material constants.

Stretch averaging: To get an average stretch versus time characteristic knowing that the tests are done at a constant displacement rate, the stretch versus time data is differentiated to get the stretch rate versus time for each series. This plot can then be compared to a constant displacement rate to identify deviations from the defined displacement rate. The time for each series is scaled by the maximum time so that all of the data have x-values between 0 and 1. Then y-values can be averaged to get a characteristic curve that is the combined average for the full range of the data. The final average for each strain rate can then be scaled by the average end time to add back the temporal aspect. After the average for each strain rate is computed, the global average is computed for all strain rates.

Stress averaging: The stretch versus time defines the displacement of the top grip with respect to the bottom; in addition, the stress versus strain characteristic must be defined for the material model. The method used here is similar to the method used for the stretch versus time averaging, in which the strains are normalized by the maximum strain for each series, and the stresses are normalized by the maximum stress for each series. The averaged stress versus strain curves for each strain rate can then be regressed to a polynomial (order depends on fit) enabling them to be scaled by the average end strain and end stress. In addition, the global stress versus

strain curve can be calculated similarly by a regression of the series. The average can then be scaled back by the average end strain and average end stress.

Material selection: After the global stretch versus time and global stress versus strain relationships are found, the curves are inputt into a standard FE coupon model with varying material models to find the material model that best matches the shape of the global averages. Any material model that is deemed a possibility for this model is run with the input curves. All hyperelastic material models in LS-Dyna are considered as candidates. The different material models are compared with the target stress versus strain curve to find one that best matches the behavior of the experiments (Figure 30).

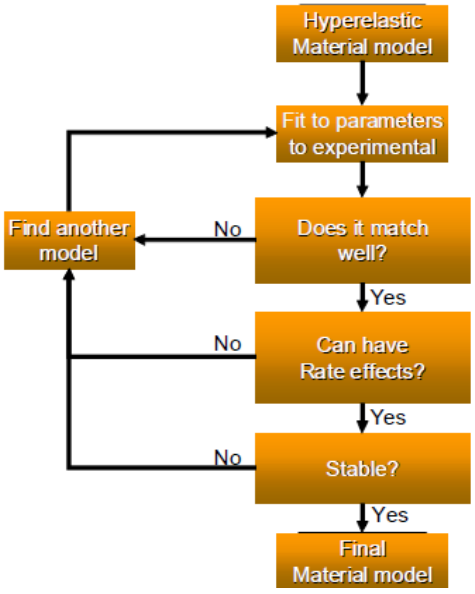

Figure 30: Methodology for selecting the appropriate material model.

Material parameter optimization: One best shape describing a material model is formulated using a polynomial from stretch and stress normalized data. Scaling parameters are defined to modify the input curve. The scaling factor approach is needed because of the need to optimize three separate loading rates, one for each strain rate, and the factors are optimized with a multi-island genetic algorithm to minimize the least square error between the model output and the target stress versus strain curve for all 3 rates (Figure 31).

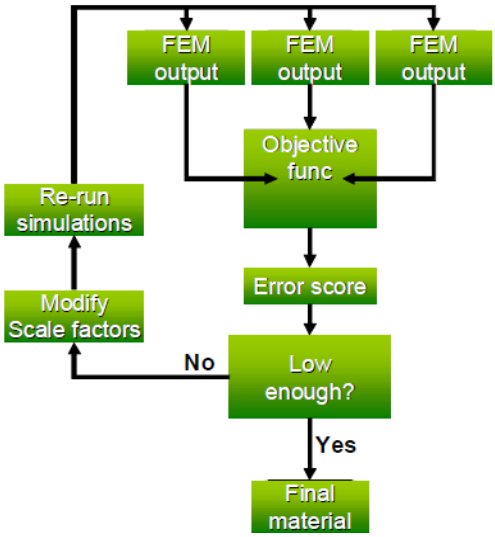

Figure 31: Methodology for optimizing the final material model.

SUMMARY

A multi-scale four step approach was utilized to characterize human liver and spleen tissue. Whole body injury analysis was performed by using the CIREN and NASS/CDS databases. Whole organ impacts were then performed. Sub-failure tests, at multiple rates, and failure tests were performed on each whole organ. Tissue level tension and compression failure tests were then performed on each organ at four different loading rates. Finally, finite element modeling was utilized to obtain an optimum model of the different tissue level tests. It is anticipated that the data from this research will enhance the understanding of internal organ injuries and provide a foundation for future human internal organs finite element models.

ACKNOWLEDGEMENTS

The authors would like to acknowledge the Toyota Motor Corporation for their funding and support.

REFERENCES

Augenstein J, Bowen J, Perdeck E, Singer M, Stratton J, Horton T, Rao A, Digges KH, Malliaris AC, Steps J. Injury Patterns in Near-Side Collisions. SAE 2000 World Congress: SAE International. 2000.

Bondy N. Abdominal Injuries in the National Crash Severity Study. National Center for Statistics and Analysis. 59-80, 1980.

Elhagediab A, Rouhana S. Patterns of Abdominal Injury in Frontal Automotive Crashes. The 16th International Technical Conference on the Enhanced Safety of Vehicles. 1998.

Hollenstein M, Nava A, Valtorta D, Snedeker JG, Mazza E. Mechanical Characterization of the Liver Capsule and Parenchyma. In: Szekely MHG, editor. Biomedical Simulation. Berlin/Heidelberg: Springer-Verlag. 150-158, 2006.

Hurtuk M, Reed R, Esposito T, Davis K, Luchette F. Trauma Surgeons Practice what the Preach: The NTDB Story on Solid Organ Injury Management. Journal of Trauma. 61(2): 243-255, 2006.

Kerdok A, Ottensmeyer M, Howe R. Effects of Perfusion on the Viscoelastic Characteristics of Liver. Journal of Biomechanics. (39): 2221-2231, 2006.

Lessley D, Crandall J, Shaw G, Funk J, Kent R. A Normalization Technique for Developing Corridors from Individual Subject Responses. SAE Technial Paper Series. Detriot, MI, 2004.

Mackenzie E, Fowler C. Epidemiology. In: Moore EE, Feliciano DV, Mattox KL, eds. Trauma. 5th ed. New York: McGraw- Hill; 21–39, 2003.

Matthews J and Martin J. Atlas of Human Histology and Ultrastructure. Philadelphia: Lea & Febiger, 1971.

Mazza E, Nava A, Hahnloser D, Jochum W, and Bajka M. The Mechanical Response of Human Liver and its Relation to Histology: An In Vivo Study. Medical Image Analysis. 11: 633-672, 2007.

Melvin J, Stalnaker R, Roberts V, Trollope M. Impact Injury Mechanisms in Abdominal Organs. Proceedings of the 17th Stapp Car Crash Conference. Society of Automotive Engineers, Warrendale, PA: 115-126, 1973.

Moorcroft D, Duma S, Stitzel J, Duma G. Computational Model of the Pregnant Occupant: Predicting the Risk of Injury in Automobile Crashes. American Journal of Obstetrics and Gynecology. 189 (2): 540-544, 2003.

Nasseri S, Bilston L, and Tanner R. Lubricated Squeezing Flow: A Useful Method for Measuring the Viscoelastic Properties of Soft Tissue. Biorheology. 40: 545-551, 2003.

Roan E, and Vemaganti K. The Non-Linear Material Properties of Liver Tissue Determined from No-Slip Uniaxial Compression Experiments. Transactions of ASME. 129: 450-456, 2007.

Santago A, Kemper A, McNally C, Sparks J, Duma S. The effect of Temperature on the Mechanical Properties of Bovine Liver. Biomed. Sci. Instrum. 45: 376-381, 2009a.

Santago A, Kemper A, McNally C, Sparks J, Duma S. Freezing Affects the Mechanical Properties of Bovine Liver. Biomed. Sci. Instrum. 45: 24-29, 2009b.

Sparks J, Bolte J, Dupaix R, Jones K, Steinberg S, Herriott R, Stammen J, Donnelly B. Using Pressure to Predict Liver Injury Risk from Blunt Impact. Stapp Car Crash Journal. 51: 401-432, 2007.

Stingl J, Baca V, Cech P, Kovanda J, Kovandova H, Mandys V, Rejmontova J, Sosna B. Morphology and some biomechanical properties of human liver and spleen. Surgical and Radiological Anatomy. 24(5): 285-289, 2002.

Stitzel J, Gayzik F, Joth J, Mercier J, Gage D, Morton K, Duma S, Payne R. Development of a Finite Element-Based Injury Metric for Pulmonary Contusion Part I: Model Development and Validation. Stapp Car Crash Journal. 49: 271-289, 2005a.

Stitzel J, Hansen G, Herring I, Duma S. Blunt Trauma of the Aging Eye: Injury Mechanisms and Increasing Lens Stiffness. Archives of Ophthalmology. 123: 789-794, 2005b.

Takhounts E, Ridella S, Tannous R, Campbell J, Malone D, Danelson K, Stitzel J, Rowson S, Duma S. Investigation of Traumatic Brain Injuries Using the Next Generation of Simulated Injury Monitor (SIMon) Finite Element Head Model. Stapp Car Crash Journal. 52: 1-31, 2008.

Tamura A., Omori K, Miki K, Lee J, Yang K, King A. Mechanical Characterization of Porcine Abdominal Organs. Stapp Car Crash Journal. 46: 55-69, 2002.

Thor, C. “Characteristics of Thoracic Organ Injuries in Frontal Crashes.” MS Thesis

Virginia Polytechnic Institute and State University, 2008.

Uehara H. A Study on the Mechanical Properties of the Kidney, Liver, and Spleen, by Means of Tensile Stress Test with Variable Strain Velocity. Journal of Kyoto Prefectural University of Medicine. 104(1): 439-451, 1995.

Wang B, Wang G, Yan D, Liu Y. An Experimental Study on Biomechanical Properties of Hepatic Tissue Using a New Measuring Method. Bio-Medical Materials and Engineering. 2: 133-138, 1992.

Yamada H. Strength of Biological Materials. Baltimore: Williams and Wilkins, 1970.